Catalysis Today 328 (2019) 99–104

Contents lists available at ScienceDirect

Catalysis Today

journal homepage: www.elsevier.com/locate/cattod

Photocatalytic activity of ZnO nanopowders: The role of production techniques in the formation of structural defects

Igor Danilenko[a,*], Oksana Gorban[a], Pavel Maksimchuk[b], Oleg Viagin[b], Yurii Malyukin[b], Sergii Gorban[a], Galina Volkova[a], Valentina Glasunova[a], Maria Guadalupe Mendez-Medrano[c], Christophe Colbeau-Justin[d], Tetyana Konstantinova[a], Svitlana Lyubchyk[e]

[a] Donetsk Institute for Physics and Engineering, NAS of Ukraine, Kiev, 03028, Nauky, av., 46, Ukraine
[b] Institute for Scintillation Materials, NAS of Ukraine, Nauky ave. 60, Kharkiv, 61072, Ukraine
[c] Laboratoire de Physique des Interfaces et des Couches Minces, École Polytechnique, Route de Saclay, 91128 Palaiseau cedex, France
[d] Laboratoire de Chimie Physique, UMR 8000 CNRS, University Paris-Sud, University Paris-Saclay, 91405 Orsay, France
[e] NOVA ID FCT, Campus de Caparica, 2829-516, Caparica, Portugal

ARTICLE INFO

Keywords:
Photocatalytic activity
ZnO
Structure defects
Vacancies
Luminescence

ABSTRACT

The effect of the type of structural defect in zinc oxide on its photocatalytic properties was studied for phenol photodegradation under UV-irradiation. It was shown that the use of different types of precursors (zinc oxalate and zinc hydroxide) for the production of zinc oxide leads to the formation of a material with the same phase composition and equal energy of the forbidden band, but different photocatalytic activities. Simultaneously, the peculiarities of the luminescence and electron spin resonance spectra indicate the formation of different types of defects in the structure of the material, namely, oxygen vacancies (V_o) in the anionic and zinc vacancies (V_{Zn}) in the cationic sublattices of zinc oxide synthesised from the zinc oxalate and hydroxide, respectively. Also, the different characteristics of the luminescence decays reveal the different recombination paths for the free charge carriers in the systems synthesised from the different precursors. The different times of the luminescence decay also confirmed the different methods of recombination of free charge carriers in systems synthesised from different precursors. It was shown that the appearance of defects in the cationic sublattice leads to a decrease in the photocatalytic activity of the material relative to phenol degradation.

1. Introduction

Resource saving, energy efficiency and clean technologies have been recognised as priority areas of the world economy and have been intensively developing in recent years [1]. There are technologies for water purification, green energy, environmental monitoring and production processes, biomedical diagnostics and so on [2–4]. The materials determine the effectiveness of these technologies, in many ways. Photocatalytic materials are the most interesting for these applications, because they use the energy of the sun [5,6]. However, their functionality depends on the physical (the energy position of the band gap, band gap parameters, photon lifetime and so on) and the chemical properties of the material (the nature of active surface centres and the ability to generate a reactive oxygen species) [7–9].

The best-known photocatalytic material is TiO_2, especially as the material of the trademark P25 [10]. Its photocatalytic activity is determined by the sufficient size of its band gap (3.2 eV) and the appropriate position of its conduction and valence bands for oxidation-reduction processes, with the generation of reactive oxygen species and the oxidation of organic pollutants [11,12]. Simultaneously, the catalytic activity of TiO_2 is determined by the presence of a surface of active centres of the Lewis nature, basic (-Ti = O) or acidic ($Ti^{\delta+}$), on which molecular oxygen and organic pollutants can be adsorbed [13,14]. The synergism of the photo- and catalytic activity of this material determines its high functionality, especially in the process of water purification from pollutants that are hard bases according to Pearson's theory [15]. However, for the processes of the antibacterial treatment of water and air, when the pollutants have functional groups of soft Pearson's bases also, the boarding or soft Pearson's metal oxides as photocatalytic materials are also very interesting [16–18]. On this basis, ZnO is an attractive material, because it has practically the same width and position of the band gap as in TiO_2, but within Pearson's theory, zinc ions are described as boarding acids [16].

Recently, several reviews have been published on the photocatalytic

* Corresponding author.
E-mail addresses: danilenko.i@nas.gov.ua, igord69@ukr.net (I. Danilenko).

https://doi.org/10.1016/j.cattod.2019.01.021
Received 7 July 2018; Received in revised form 31 December 2018; Accepted 7 January 2019
Available online 08 January 2019
0920-5861/

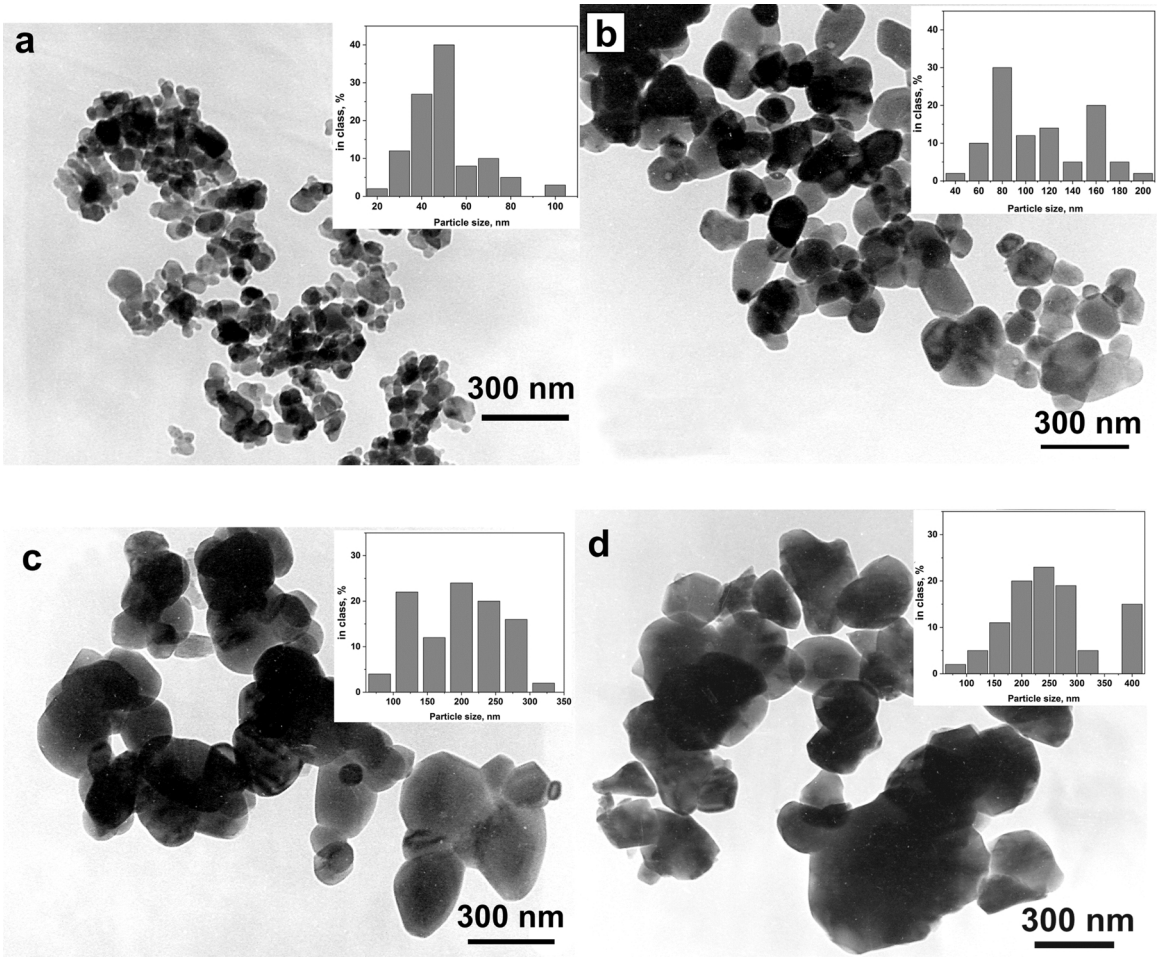

Fig. 1. TEM images of ZnO nanoparticles synthesised by chemical precipitation from: zinc oxalate – a, c) and zinc hydroxide – b, d) and fired at 500 °C – a, b) and 700 °C – c, d). In the inserts the particle size distribution according TEM data are shown.

activity of ZnO in various processes [17–21]. The defects in the structure of ZnO, as a semiconductor material for photovoltaics and optoelectronics, have been studied in detail in terms of zone structure and their influence on the functional properties of the material [22–24]. Several types of defects are distinguished in the structure of ZnO, namely, interstitial zinc atoms (Zn_i) or oxygen (O_i), as well as vacancies in the sites of the cation sublattice (V_{Zn}) or the anion sublattice (V_o) [25,26]. The formation of defects in the structure of ZnO leads to the appearance of energy levels of the donor or acceptor type in the forbidden band [27]. These centres take part in processes that occur during photoexcitation of the system [28]. Alternatively, using chemical terminology, it is possible to describe a defective structure of ZnO with oxygen vacancies on the surface as a Lewis acid, while a defective structure with zinc vacancies can be described as a Lewis base [29]. However, the complex impact of the structural components on the efficiency of the photocatalyst is often not taken into account but only the chemical and phase compositions of the different photocatalysts are compared [30]. Therefore, in order to understand the effect of the structural peculiarities of a material on its photocatalytic activity, the same material with the same chemical and phase composition but with different types of defects will be studied in this work.

2. Experimental

ZnO nanoparticles were synthesized using a precipitation technique from $ZnCl_2$ salt. As a precipitant the water solutions of ammonium hydroxide and oxalic acid were used. All used chemicals were of chemical purity. The gel-like precipitates were obtained by the addition of an aqueous solution of $ZnCl_2$ in water solution of NH_4OH or oxalic acid with continuously stirring for 30 min. The precipitates were recovered by suction filtration using a vacuum pump. The sediments residue was washed several times with distilled water before drying in a microwave furnace (P = 700 W, f = 2.45 GHz). The dried hydroxides were calcined in a resistive furnace at 500 and 700 °C with a dwell time of 2 h [31].

The powders were characterized by means of X-ray diffraction (XRD) with Cu-Kα radiation for crystallite sizes and quantitative phase analyses. The crystallite size (D) for the synthesized ZnO nanoparticles is calculated using Debye Scherrer's equation [32]:

$$D = K\lambda/\beta_g \cos\theta,$$

where λ is the wavelength of radiation used, θ is the Bragg angle and $K = 0.9$ for spherical shape. Particle sizes of different calcined powders were estimated by means of transmission electron microscopy (TEM) (JEM 200, Jeol, Japan). The optical properties of ZnO nanopowders were measured on a Cary 5000 UV–vis-NIR spectrometer (Agilent Technologies, USA). For the determination of band gap, the following relational expression proposed by Tauc, Davis and Mott is used [33]:

$$(h\nu F(R))^{1/n} = A(h\nu - Eg),$$

where h - Planck's constant, ν - frequency of vibration, $F(R) = (1-R)^2/2R$- Kubelka-Munk function, R - is the absolute reflectance of the sampled layer, Eg - band gap, A - proportional constant. The value of the exponent n denotes the nature of the sample transition and for direct allowed transition n = ½.

The electron spin resonance (ESR) investigation was carried out on ESR spectrometer CMS-8400 (Adani, Belarus) at room temperature. Luminescence spectra of different kinds of ZnO powders were obtained using LUMINA fluorescence spectrometer (Thermo Scientific, USA). The technique of the time-correlated single photon counting was used to study the lifetime of the defects excited states in the ZnO. Decay curves were measured by the TimeHarp 260 NANO system and the single photon detector PMA 182 (PicoQuant, Germany). An excitation of luminescence was induced by the third harmonic (355 nm) of the Nd:YAG pulsed laser (NL202 model, EKSPLA, Lithuania).

The photocatalytic activity of the ZnO nanoparticles was tested by photodegradation of phenol used as model pollutant in water with concentration of 50 ppm under UV-illumination. Before UV irradiation, the photocatalyst was dispersed in the water-phenol solution by sonication for 120 s and then by magnetic stirring for 10 min in the dark to ensure equilibrium between adsorption and desorption. The solution was irradiated using a Heraeus Noblelight Peschl Ultraviolet Reactor LRS1 with a medium pressure UV lamp TQ 150 (150 W). The tests were carried out in 400 mL water cooled reactor containing 350 mL of the phenol-water solution and 0.9 g/L of photocatalyst. The principle of sample preparation technique was described in [34]. The powder was separated by filtration and then the resultant transparent solution was analysed by High Performance Liquid Chromatography (HPLC, Agilent 1260) equipped with a UV-detector set at 260 nm for phenol analysis.

3. Results and discussion

3.1. TEM and XRD studies

Fig. 1 shows the TEM images of ZnO nanoparticles synthesised by chemical precipitation from different precursors, namely, ZnC_2O_4 (Fig. 1a and c) and $Zn(OH)_2$ (Fig. 1b and d), and fired at different temperatures of 500 and 700 °C.

The nature of the precursor effects on the morphology of the ZnO powders synthesised with 500 °C calcination. The use of ZnC_2O_4 as precursor material results in the formation of finer and more dispersed ZnO particles. The average particle size of ~30 nm and an average aggregate size of ~100 nm was determined. The use of $Zn(OH)_2$ as a precursor material results in the formation of a larger particles (an average size of 50 nm) aggregated in groups with an average size of ~300 nm. An increase of the synthesis temperature to 700 °C practically neutralises the effect of the precursor on the morphological characteristics of the synthesised ZnO powders and the average particle size is ~200–300 nm.

The XRD data for ZnO powders synthesised from both types of precursors are shown in Fig. 2a. It was shown that, regardless of the type of precursor used for synthesis, ZnO crystallised in the wurtzite structure, P63mc. XRD data show that the coherent scattering areas of ZnO synthesised from ZnC_2O_4 were 32 and 47 nm after calcination at 500 and 700 °C, respectively, and for ZnO synthesised from $Zn(OH)_2$ were 47 and 48 nm after calcination at 500 and 700 °C, respectively. The formation of smaller particles of ZnO after calcination at low temperatures of ZnC_2O_4 may be caused by chelating effect of oxalate chains [35–37] in comparison with $Zn(OH)_2$.

3.2. Optical and luminescent properties

The UV–vis diffuse reflectance spectra for ZnO synthesised from different precursors shown that the optical band gap for ZnO prepared from ZnC_2O_4 is 3.23 eV and for ZnO prepared from $Zn(OH)_2$ is 3.2–3.21 eV (Fig. 2b). Therefore, the materials with practically identical band gap were synthesised.

The luminescence spectra of ZnO powders synthesised from oxalate and hydroxide precursors are different (Fig. 3). In the luminescence spectrum of the ZnO nanopowder synthesised from ZnC_2O_4, a green luminescence band (λ = 510 nm) was observed, while a red luminescence band (λ = 650 nm) was found in the spectrum of the ZnO nanopowder synthesised from $Zn(OH)_2$. This indicates the presence of various defects in the structure of ZnO synthesised from different precursors [38]. The latest studies describing the luminescence spectra in ZnO consisting of Zn-enriched ($Zn_{1+\delta}O$) and Zn-depleted ($Zn_{1-\delta}O$) zinc oxide systems [39,40] have made it possible to relate the type of material defect to its luminescent properties more precisely. According to the studies [39,41], the presence of green emission is generally linked to the transition between a singly charged oxygen vacancy (vacancy with localized state) and a photo-excited hole in a valence band. Whereas, an additional appearance of zinc vacancies in the system leads to the donor-acceptor mechanism of luminescence (V_o-V_{Zn}) and leads to the appearance the yellow-orange and red bands in the luminescence spectrum [42].

The decay curves of the luminescence band with λ_{max} = 510 nm are in the microsecond range, while the decay curves of the luminescence band with λ_{max} = 650 nm are in the millisecond range. In both cases the decay curves are non-exponential, but are different from each other. The shape of the decay curves of the red band is very close to hyperbola. The hyperbolic decay may be due to various processes including trapping/retrapping of the charge carriers, recombination between deep donors and acceptors, etc [43]. Such processes are characterized by hyperbolic decay of different orders. The order of the hyperbola can be obtained by plotting decay curves in double logarithmic scale and determining their slopes (inserts in Fig. 3 a, b). For the curves at the insert in Fig. 3b, the slope is almost equal to unit, so the decay of the red luminescence of the samples from $Zn(OH)_2$ corresponds to a first order hyperbola. This indicates that the red band at 650 nm is due to the single process of donor-acceptor recombination [43]. Simultaneously, the decay curves of the green band of ZnO from ZnC_2O_4 are more complicated and cannot be fitted by an exponential or hyperbolic law

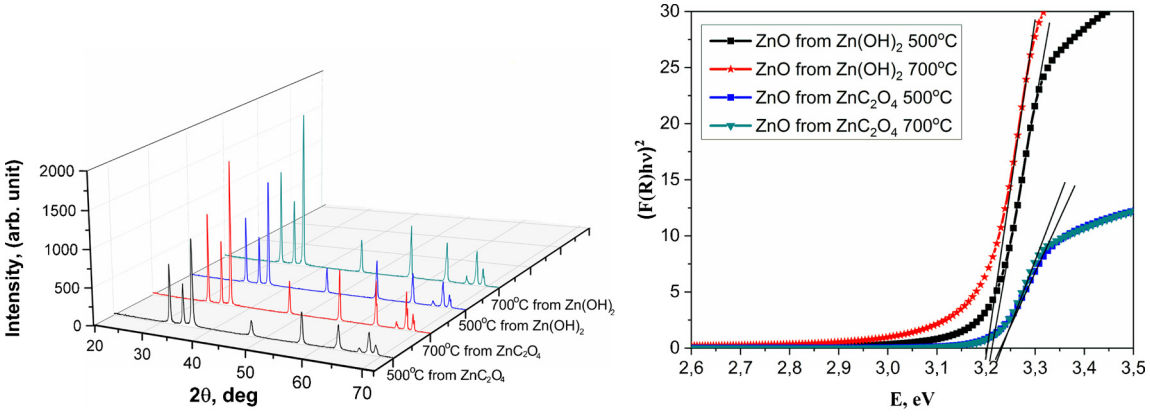

Fig. 2. XRD – a) and DRS – b) data for zinc oxide synthesised from zinc oxalate and zinc hydroxide precursors.

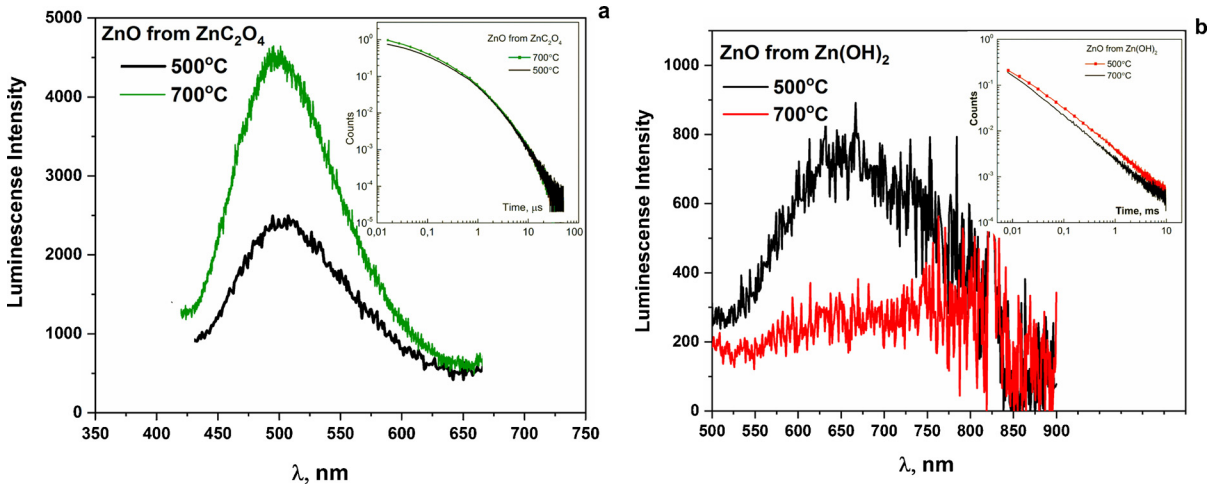

Fig. 3. Luminescence spectra of the zinc oxide nanopowders synthesised from: a) ZnC_2O_4, b) $Zn(OH)_2$ and calcined at 500 and 700 °C; on the inserts the decay curves in double logarithmic scales for all types of systems at λ_{ex} = 355 nm: c) λ_{reg} = 510 nm, d) λ_{reg} = 650 nm.

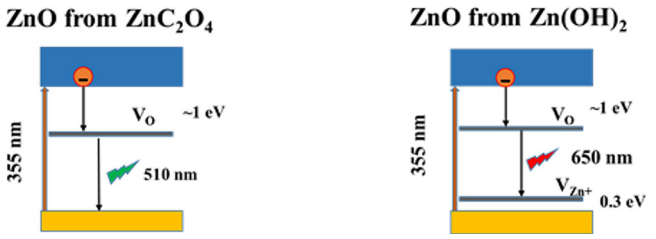

Fig. 4. Schematic illustration of different defect levels in ZnO powders, obtained from ZnC_2O_4 and $Zn(OH)_2$, which are responsible for the PL emission of different wavelength.

(insert on Fig. 3a). As shown in [43], such a form of the decay curves is determined by several processes involving the radiative decay of the luminescence centre, as well as the kinetics of the release of charge carriers from the traps. According to our PL investigation and literature data [44,45] we can to propose the next schemes of the energy levels diagram showing the position of the defect levels in ZnO in our case. (Fig. 4).

The formation of V_O and V_{Zn} defects in ZnO synthesised from ZnC_2O_4 and $Zn(OH)_2$, respectively, is caused by the peculiarities of chemical transformations of ZnC_2O_4 and $Zn(OH)_2$ during the thermal decomposition.

The formation of ZnO with oxygen vacancies ($ZnO_{1-\delta}$) occurs during the ZnC_2O_4 decomposition in air at the temperatures above 450 °C according to the next reaction:

$$Zn(COO)_2 = ZnO + CO_2 + CO,$$

and then the partially reduction of ZnO under CO atmosphere according to the reaction:

$$ZnO + \delta CO = ZnO_{1-\delta} + \delta CO_2,$$

and led to form a Zn-enriched precipitate of ZnO with oxygen vacancies ($ZnO_{1-\delta}$).

Simultaneously, the production of $Zn(OH)_2$ in an ammonium solution at pH > 8 leads to the formation of $Zn(OH)_2$ with zinc hydroxocomplexes ($Zn(OH)_n^{2-n}$) adsorbed on the surface with a large amount of water and hydroxyls in the structure [46,47]. The next reaction occurs at heat-treatment of such systems – $Zn(OH)_2 = ZnO + 2H_2O$, $Zn(OH)_n^{2-n} = ZnO + H_2O + (2\text{-}n)OH^-$. The follow condensation of some amount surface adsorbed OH_s- groups led to condensation reaction - $2\delta OH_s = \delta H_2O + \delta O^{2-}$ (as results the δ surplus lattice O^{2-} ions are created). It may be concluded that the decomposition of $Zn(OH)_2$ with surface adsorbed oxygen-rich hydrocomplexes above 350 °C leads to the creation of O-rich ($ZnO_{1+\delta}$) or another words the Zn-depleted oxide ($Zn_{1-\delta}O$).

3.3. Electron spin resonance spectroscopy data

The ESR spectra of ZnO powders synthesised from both precursors are shown in Fig. 5. The ESR spectra of ZnO particles synthesised from ZnC_2O_4 and calcined at different temperatures did not contain any signals. The ESR spectra generated from the ZnO powder prepared from $Zn(OH)_2$ and calcined at 500 °C demonstrates a signal with **g** = 2.0024. The signal with such a **g**-factor corresponds to charged Zn vacancies (V_{Zn}^-) or the V_{Zn}^--Zn_i complex [44,45,48–51]. To understand the creation of this type of ESR signal, the $Zn(OH)_2$ precursors heated at 200 and 400 °C were also investigated by ESR spectroscopy. It was shown that after calcination at 200 °C, the ESR spectrum contains a signal with **g** = 1.9567 that corresponds to the shallow levels of oxygen vacancy (V_o^+) and a weak signal with **g** = 2.0024 that corresponds to zinc vacancies (V_{Zn}^-) [27,41]. The increasing of the calcination temperature to 400–500 °C leads to the disappearance of the ESR signal with **g** = 1.9567 and an increase in the intensity of the ESR signal with **g** = 2.0024 (V_{Zn}^-). The peculiarities of the synthesis process of ZnO from the $Zn(OH)_2$ may explain such behaviour of the ESR signals. The appearance of surface V_o^+ (donor levels) results from the OH-group removal with heat treatment at 200 °C. At the same time, a number of V_{Zn}^- appeared in O-rich systems during calcination. Heat treatment at

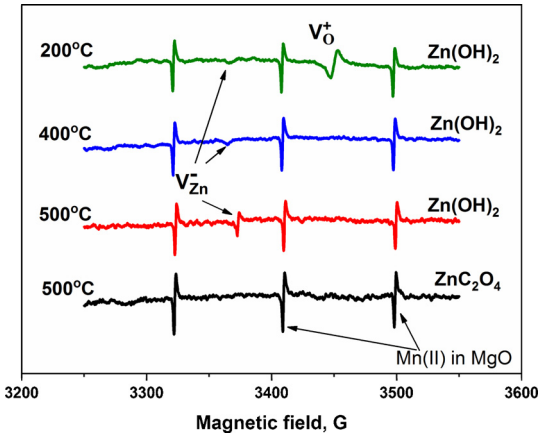

Fig. 5. ESR signals of ZnO powders, synthesized from different precursors and calcined at different temperatures. Reference peaks Mn(II) in cubic MgO is shown.

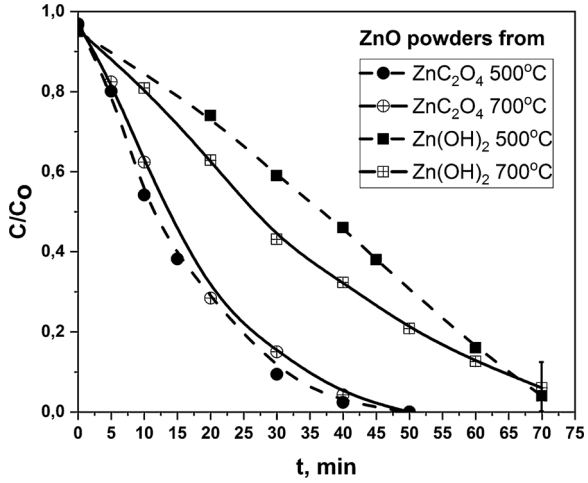

Fig. 6. Photocatalytic degradation of phenol in presence of ZnO nanoparticles synthesised from different precursors.

higher temperatures leads to the rebuilding of the crystal structure from $Zn(OH)_2$ to ZnO, resulting in a decrease in the amount of oxygen surface V_o^+ and the accumulation of V_{Zn}^- (Fig. 5).

ESR spectrum of ZnO, that was obtained by oxalate technology, did not show the ESR signals from as single ionized zinc vacancies (V_{Zn}-) and as oxygen vacancies (V_{o+}). It may be as results healing of oxygen vacancies to low concentration below detection limit [52] for system with a high calcination temperature. It is known that the experimental detection of centres with S = 1, in particular neutral oxygen vacancies Vo or double ionized oxygen vacancies (V_{O2+}) cannot measured by ESR spectroscopy. The PL spectra of these systems show the presence of green luminescence peak at 510 nm (2.4 eV). According to [53,54] that the transition of an electron from the conduction band to V_{o+} level cannot yield photons with energy of 2 eV and only recombination of a conduction band electron with a V_{O2+} center can yield photons with an energy of about 2 eV. Additionally, as it is shown in [52,55,56] the emission in ZnO due to double ionized oxygen vacancies has lower energy than in case of the emission due to the recombination of the electron trapped in singly ionized oxygen vacancies with photo generated holes. Thus, we can conclude that green emission at 510 nm in PL spectra of ZnO may be attribute to Vo_{2+} presence in ZnO.

3.4. Photocatalytic activity of ZnO

The normalised concentration of phenol (C/C_o) versus illumination time is shown in Fig. 6. It has be found that the ZnO prepared from the ZnC_2O_4 shows the higher photocatalytic activity than ZnO synthesised from the $Zn(OH)_2$. The difference in the photocatalytic properties of ZnO synthesised from different precursors can be attributed to the different nature of defects in ZnO formed in these synthetic approaches: some kinds of the oxygen vacancies (V_o, V_o^+ and V_o^{2+}) for the first case and V_{Zn}^- for the second case. Possible reactions that occur during the phenol (PhOH) degradation in solution in the presence of a photocatalyst (PC) are presented below. The oxygen vacancy on the ZnO surface corresponds to a Lewis acid centre, and the O^{2-} ions on the surface correspond to Lewis basic centres. Under the influence of UV-irradiation, the electron-hole pairs are generated, the electron enters the conduction band and a hole is formed in the valence band (**PC + hv = h^+ + e-**). The second process may proceed when the charges are captured by various surface or lattice defects. The electron is captured by the oxygen molecule adsorbed on the Lewis acid centre of PC and formed the superoxide anion radical (**PC + O_2 = PC…O_2 = PC + …O_2-**). The hole can be captured either by lattice O^{2-} with the formation of an O- centre on the surface (**h^+ + O_s^{2-} = O-$_s$**) or an OH-group with the formation of an OH· radical. The interaction of active sites with phenol leads to the formation of complexes and facilitates the degradation of phenol (**PhOH + ZnO = PhOH…(LA…O_2-)ZnO** or **PhOH + ZnO = PhOH….(O-$_s$)ZnO**). Our experience for PhOH degradation in the presence of set of photocatalysts (P25, ZnO) but without oxygen in reaction medium occurs only up to 20% that is very good agreements with other studies [57]. The crucial role of O_2- in PhOH degradation are described in many work [58,59] and it may be present as electron scavenger for enhanced of charge separation in PC and also as the oxidative agent for PhOH and different intermediates. The interaction of the formed centres with the water molecule leads to the generation of other forms of active oxygen - peroxide and hydroxyl radicals, which can diffuse from the surface into the solution, (**ZnO/O_2-…H_2O = H_2O_2 (2OH·)** or **ZnO/O-….H_2O = OH- (OH·)**) and participate in the reactions of phenol oxidation (**PhOH….ZnO = CO_2 + H_2O**).

Thus, the formation of the super anion oxide radical is an important feature for the high photocatalytic activity of the material. Since, it leads to an effective charge separation, and forms an active oxygen adsorbed onto Lewis acid centre of the ZnO surface. This explains why ZnO formed from ZnC_2O_4 has a higher photocatalytic activity.

4. Conclusions

The effect of two different precursor materials (zinc oxalate and zinc hydroxide) on the structural peculiarities of ZnO powders and their catalytic activity was studied. It was shown that both materials with the same phase composition and with the same band gap demonstrate different photocatalytic activities. At the same time, the analysis of luminescent and ESR spectra allows us to conclude that the precursor materials effect on the nature of the structural defects of ZnO. A ZnO with oxygen vacancies was formed when ZnC_2O_4 raw material was used during precipitation, while ZnO with zinc vacancies was formed when $Zn(OH)_2$ raw material was used during precipitation. The previously formed ZnO structure differences leads to a difference in their photocatalytic activity while other experimental conditions and materials properties are equal (synthesis temperature, phase composition and width of the band gap). It was shown that ZnO with oxygen vacancies is more effective as a photocatalyst for phenol degradation. The decrease in the photocatalytic activity of ZnO with zinc vacancies is due to both factors, namely, a less efficient charge separation and a decrease in the concentration of reactive oxygen species involved in the phenol degradation reaction.

Acknowledgements

The authors are thankful the H2020-MSCA-RISE-2015 Programme, project N 690968 NANOGUARD2AR for support of this work.

References

[1] IRENA, REthinking Energy, Accelerating the Global Energy Transformation, Abu Dhabi, (2017).
[2] S.K. Misra, N.K. Pandey, V. Shakya, A. Roy, IEEE Sens. J. 15 (2015) 3582–3589.
[3] S. Nahar, M.F.M. Zain, A.A.H. Kadhum, H.A. Hasan, Md.R. Hasan, Materials. 10 (2017) 629–654.
[4] A.G. Gutierrez-Mata, S. Velazquez-Martínez, A. Álvarez-Gallegos, M. Ahmadi, J.A. Hernández-Pérez, F. Ghanbari, S. Silva-Martínez, Int. J. Photoenergy 2017 (2017) 1–27.
[5] J. Schneider, M. Matsuoka, M. Takeuchi, J. Zhang, Y. Horiuchi, M. Anpo, D.W. Bahnemann, Chem. Rev. 114 (2014) 9919–9986.
[6] M.E. Borges, M. Sierra, E. Cuevas, R.D. García, P. Esparza, Sol. Energy 135 (2016) 527–535.
[7] F. Opoku, K.K. Govender, C.G.C.E. van Sittert, P.P. Govender, Adv. Sustain. Syst. (2017) 1700006.
[8] G. Martra, Appl. Cat. A Gen. 200 (2000) 275–285.
[9] T. Jafari, E. Moharreri, A.S. Amin, R. Miao, W. Song, S.L. Suib, Molecules 21 (2016) 1–29.
[10] S.M. Gupta, M. Tripathi, Phys. Chem. 56 (2011) 1639–1657.
[11] A.L. Linsebigler, G. Lu, J.T. Yates, Chem. Rev. 95 (1995) 735–758.
[12] A.O. Ibhadon, P. Fitzpatrick, Catalysts 3 (2013) 189–218.
[13] A. Corma, H. Garcıa, Chem. Rev. 102 (2002) 3837–3892.
[14] V. Augugliaro, M. Bellardita, V. Loddo, G. Palmisano, L. Palmisano, S. Yurdak, J.

Photochem. Photobiol. C Photochem. Rev. 13 (2012) 224–245.
[15] B. Saville, Angew. Chem. Int. Ed. Eng. 6 (1967) 928–939.
[16] R.G. Pearson, Inorg. Chem. 27 (1988) 734–745.
[17] C.B. Ong, L. Yong, A.W. Mohammad, Renew. Sust. Energ. Rev. 81 (2018) 536–551.
[18] A. Sirelkhatim, S. Mahmud, A. Seeni, N. Kaus, L.C. Ann, S. Bakhori, H. Hasan, D. Mohamad, Nano-Micro Lett. 7 (2015) 219–242.
[19] K.M. Lee, C.W. Lai, K.S. Ngai, J.C. Juan, Water Res. 88 (2016) 428–448.
[20] S.D. Lee, S. Nam, M. Kim, J. Boo, Phys. Proc 32 (2012) 320–326.
[21] S. Khanchandani, P.K. Srivastava, S. Kumar, S. Ghosh, A.K. Ganguli, Inorg. Chem. 53 (2014) 8902–8912.
[22] A. Janotti, C.G. van de Walle, Rep. Prog. Phys. 72 (2009) 126501.
[23] V. Ischenko, S. Polarz, D. Grote, V. Stavarage, K. Fink, M. Driess, Adv. Funct. Matter. 15 (2005) 1945–1954.
[24] H. Kaftelen, K. Ocakoglu, R. Thomann, S. Tu, S. Weber, E. Erdem, Phys. Rev. B 86 (2012) 014113.
[25] A.M. Gsiea, J.P. Goss, P.R. Briddon, R.M. Al-habashi, K.M. Etmimi, K.A.S. Marghani, Int. J. Math. Comp. Phys. Elect. Comp. Eng. 8 (2014) 127–132.
[26] F. Oba, S.R. Nishitani, S. Isotani, H. Adachi, I. Tanaka, J. Appl. Phys. 90 (2001) 824–828.
[27] A.B. Djurišić, W.C.H. Choy, V.A.L. Roy, Y.H. Leung, C.Y. Kwong, K.W. Cheah, R.T.K. Gundu, W.K. Chan, H.F. Lui, C. Surya, Adv. Funct. Mater. 14 (2004) 856–864.
[28] F. Liu, Y.H. Leung, A.B. Djurišić, A. Ng, W.K. Chan, Phys. Chem. C 117 (2013) 12218–12228.
[29] B. Zhai, Y.M. Huang, Optoelectron. Mater. Devices 1 (2016) 22–36.
[30] D. Chen, Z. Wang, T. Ren, H. Ding, W. Yao, R. Zong, Y. Zhu, J. Phys. Chem. C 118 (2014) 15300–15307.
[31] I. Danilenko, O. Gorban, A. Shylo, L. Akhkozov, M. Lakusta, T. Konstantinova, Mater. Sci. Eng. 213 (2017) 012016.
[32] M.K. Debanath, S. Karmakar, Mater. Lett. 111 (2013) 116–119.
[33] B.D. Viezbicke, S. Patel, B.E. Davis, D.P. Birnie III, Phys. Status Solidi B 252 (2015) 1700–1710.
[34] M.G. Mendez-Medrano, E. Katarzyna-Kowalska, A. Lehoux, A. Herissan, B. Ohtani, D.B. Uribe, C. Colbeau-Justin, J.L.R. Lopez, H. Remita, V. Briois, J. Phys. Chem. C 120 (2016) 5143–5154.
[35] N. Nolan, M. Seery, S. Pillai, Chem. Mater. 23 (2011) 1496–1504.
[36] M. Kim, Y. Kim, W. Kwon, S. Yoon, Sci. Rep-UK 6 (2019) 19282, https://doi.org/10.1038/srep19282.
[37] M. Thirumavalavan, K. Huang, J. Lee, Materials 6 (2013) 4198–4212.
[38] K. Vanheusden, W.L. Warren, C.H. Seager, D.R. Tallant, J.A. Voigt, B.E. Gnade, J. Appl. Phys. 79 (1996) 7983–7987.
[39] Ü. Özgür, Ya.I. Alivov, C. Liu, A. Tekeb, M.A. Reshchikov, S. Doğanc, V. Avrutin, S.-J. Cho, H. Morkoç, J. Appl. Phys. 98 (2005) 041301.
[40] K.E. Knutsen, A. Galeckas, A. Zubiaga, F. Tuomisto, G.C. Farlow, B.G. Svensson, A.Y. Kuznetsov, Phys. Rev. B 86 (2012) 121203.
[41] K. Vanheusden, C. Seager, W. Warren, D. Tallant, J. Voigt, Appl. Phys. Lett. 68 (1996) 403–408.
[42] N.S. Norberg, D.R. Gamelin, J. Phys. Chem. B 109 (2005) 20810.
[43] K.A. Chernenko, L. Grigor'eva, E.I. Gorokhova, P.A. Rodnyi, Opt. Spectrosc. 118 (2015) 425–430.
[44] D. Das, P. Mondal, RSC Adv. 4 (2018) 35735–35743.
[45] M.N.H. Liton, M.K.R. Khanb, M.M. Rahman, M.M. Islam, J. Sci. Res 7 (2015) 23–34.
[46] N. Uekawa, R. Yamashita, Y.J. Wu, K. Kakegawa, Phys. Chem. Chem. Phys. 6 (2004) 442–446.
[47] D. Levy, E. Castellón. 2018 Wiley VCH Verlag GmbH&Co KGaA, Boschstr, 12, 69469 Weinheim Germany. P. 392.
[48] I. Shalish, H. Temkin, V. Narayanamurti, Phys. Rev. B 69 (2004) 245401.
[49] D. Galland, A. Herve, Phys. Lett. A 33 (1970) 1–2.
[50] D. Galland, A. Herve, Solid State Commun. 14 (1974) 953–956.
[51] S.B. Zhang, S.H. Wei, A. Zunger, Phys. Rev. B 63 (2001) 075205.
[52] R.N. Aljawfi, M.J. Alam, F. Rahman, S. Ahmad, A. Shahee, S. Kumar, Arab. J Chem. (2018), https://doi.org/10.1016/j.arabjc.2018.04.006.
[53] A. van Dijken, E.A. Meulenkamp, D. Vanmaekelbergh, A. Meijerink, J. Phys. Chem. B 104 (2000) 1715–1723.
[54] F.A. Kro¨ger, The Chemistry of Imperfect Crystals, North-Holland Publishing Company, Amsterdam, 1964, p. 691.
[55] U. Ozgur, Ya. Alivov, C. Liu, A. Teke, M.A. Reshchikov, S. Dogan, A. Avrutin, S.-J. Cho, H. Morko, J. Appl. Phys. 98 (2005) 041301103.
[56] M. Ghosh, A.K. Raychaudhuri, Nanotechnology 19 (2008) 445704.
[57] H. Gomez, F. Orellana, H. Lizama, H.D. Mansilla, E.A. Dalchiele, J. Chil. Chem. Soc. 51 (2006) 1006–1009.
[58] I. Wysocka, E. Kowalska, K. Trzcinsk, M. Łapinski, G. Nowaczyk, A. Zielinska-Jurek, Nanomaterials 8 (2018) 2–20.
[59] M.P. Kobylański, P. Mazierski, A. Malankowska, M. Kozak, M. Diak, M.J. Winiarski, A. Zaleska-Medynska, Surf. Interfaces 12 (2018) 179–189.